Virus-induced inflammasome activation is suppressed by prostaglandin D_2/DP1 signaling

Rahul Vijay[a], Anthony R. Fehr[b], Ann M. Janowski[a], Jeremiah Athmer[b], Dorthea L. Wheeler[a], Matthew Grunewald[b], Ramakrishna Sompallae[c], Samarchith P. Kurup[b], David K. Meyerholz[d], Fayyaz S. Sutterwala[a,e,1], Shuh Narumiya[f], and Stanley Perlman[a,b,2]

[a]Interdisciplinary Program in Immunology, University of Iowa, Iowa City, IA 52242; [b]Department of Microbiology, University of Iowa, Iowa City, IA 52242; [c]Iowa Institute of Human Genetics, University of Iowa, Iowa City, IA 52242; [d]Department of Pathology, University of Iowa, Iowa City, IA 52242; [e]Department of Internal Medicine, University of Iowa, Iowa City, IA 52242; and [f]Department of Pharmacology, Kyoto University Faculty of Medicine, Tokyo, Japan 606-8501

Edited by Diane E. Griffin, Johns Hopkins Bloomberg School of Public Health, Baltimore, MD, and approved May 31, 2017 (received for review March 10, 2017)

Prostaglandin D2 (PGD_2), an eicosanoid with both pro- and anti-inflammatory properties, is the most abundantly expressed prostaglandin in the brain. Here we show that PGD_2 signaling through the D-prostanoid receptor 1 (DP1) receptor is necessary for optimal microglia/macrophage activation and IFN expression after infection with a neurotropic coronavirus. Genome-wide expression analyses indicated that PGD_2/DP1 signaling is required for up-regulation of a putative inflammasome inhibitor, PYDC3, in $CD11b^+$ cells in the CNS of infected mice. Our results also demonstrated that, in addition to PGD_2/DP1 signaling, type 1 IFN (IFN-I) signaling is required for PYDC3 expression. In the absence of *Pydc3* up-regulation, IL-1β expression and, subsequently, mortality were increased in infected $DP1^{-/-}$ mice. Notably, survival was enhanced by IL1 receptor blockade, indicating that the effects of the absence of DP1 signaling on clinical outcomes were mediated, at least in part, by inflammasomes. Using bone marrow-derived macrophages in vitro, we confirmed that PYDC3 expression is dependent upon DP1 signaling and that IFN priming is critical for PYDC3 up-regulation. In addition, *Pydc3* silencing or overexpression augmented or diminished IL-1β secretion, respectively. Furthermore, DP1 signaling in human macrophages also resulted in the up-regulation of a putative functional analog, POP3, suggesting that PGD_2 similarly modulates inflammasomes in human cells. These findings demonstrate a previously undescribed role for prostaglandin signaling in preventing excessive inflammasome activation and, together with previously published results, suggest that eicosanoids and inflammasomes are reciprocally regulated.

coronavirus | inflammasomes | pyrin domain-only protein | encephalitis | prostaglandin D2

Small eicosanoids, including prostaglandins, are critical molecules in the initiation, propagation, and resolution of inflammation. In one instance, inflammasome activation by flagellin resulted in eicosanoid dysregulation (an "eicosanoid storm") with hyperinflammatory responses and rapid lethality (1, 2). Conversely, eicosanoids have been reported both to inhibit and to enhance inflammasome activation (3–7), although the precise mechanisms leading to each outcome are not well understood. Further, type I IFN (IFN-I), another key component of the innate immune response, also inhibits exuberant IL-1β expression (8, 9). Controlled IL-1β expression and function are especially important in the CNS, where the overexpression of IL-1β has been associated with neuronal damage (10).

Prostaglandins initiate signaling through multiple receptors and may have both proinflammatory and resolving/anti-inflammatory effects, depending in part on the specific receptor they engage. Prostaglandin D2 (PGD_2), the most abundant prostaglandin in the brain (11), is considered anti-inflammatory when it signals through the D-prostanoid receptor 1 (DP1 receptor) present on myeloid cells but proinflammatory when it binds to the DP2/CRTH2 receptor on Th2 CD4 T cells (12, 13). PGD_2/DP1 signaling, which triggers G protein activation and cAMP production, has been associated with diverse functions, including neuroprotection after ischemia, astrogliosis and demyelination in *twitcher* mice, damage after spinal cord contusion injury, and regulation of the sleep–wake cycle (14–19). In addition, a PGD_2 derivative, 15d-PGJ_2, also signals through the DP1 receptor, inhibiting the inflammatory response (4). Considering the multifarious effects of the PGD_2/DP1 axis and the relative abundance of PGD_2 in the brain, we reasoned that DP1 signaling would contribute to the regulation of the CNS-specific response to pathogens.

To examine this possibility, we infected mice genetically deficient in DP1 receptor expression (*PTGDR1*$^{-/-}$ mice, called "$DP1^{-/-}$" herein) with a neurotropic virus, mouse hepatitis virus strain JHM (herein, "MHV"). MHV causes acute encephalitis and chronic demyelinating encephalomyelitis. The strain of MHV that we used primarily infects oligodendrocytes, causing a sublethal encephalomyelitis (20). Infection of $DP1^{-/-}$ mice resulted in greatly increased mortality compared with WT mice. Here, we demonstrate that the lack of DP1 signaling was associated with delayed kinetics of virus clearance, diminished IFN-I production, and decreased survival. Myeloid ($CD11b^+$) cells in the CNS are comprised of two macrophage populations, resident

Significance

Inflammatory responses to viral infections must be optimized to clear the pathogen without tissue damage. Inflammasomes comprise an important component of the innate immune response. Inflammasome activity must be carefully controlled to prevent a hyperinflammatory response, especially in brain infections. Here we identify a host factor, PYDC3, that is dependent upon prostaglandin D2 (PGD_2) and IFN-I signaling and is required to modulate inflammasome activation. After infection, inflammasome activation and expression of a downstream proinflammatory cytokine, IL-1β, were increased in mice deficient in PGD_2 signaling, decreasing survival. Excess mortality was reversed by IL-1β receptor blockade. These results define a consequence of prostaglandin signaling and shed light on prostaglandin–inflammasome interactions, which modulate excessive inflammation and tissue damage in the virus-infected brain.

Author contributions: R.V., A.R.F., S.P.K., F.S.S., and S.P. designed research; R.V., A.R.F., A.M.J., J.A., D.L.W., and M.G. performed research; S.N. contributed new reagents/analytic tools; R.V., R.S., D.K.M., and S.P. analyzed data; and R.V. and S.P. wrote the paper.

The authors declare no conflict of interest.

This article is a PNAS Direct Submission.

Data deposition: The data reported in this paper have been deposited in the Gene Expression Omnibus (GEO) database, https://www.ncbi.nlm.nih.gov/geo (accession nos. GSE84653 and GSE84709).

[1]Present address: Department of Internal Medicine, Cedars-Sinai Medical Center, Los Angeles, CA 90048.

[2]To whom correspondence should be addressed. Email: stanley-perlman@uiowa.edu.

This article contains supporting information online at www.pnas.org/lookup/suppl/doi:10.1073/pnas.1704099114/-/DCSupplemental.

microglia/macrophages and infiltrating macrophages. Our results demonstrated that DP1 signaling was required for optimal expression of pyrin domain (PYD) only-containing protein 3, PYDC3, in $CD11b^+$ cells in the MHV-infected CNS with the most profound effects in microglia. Inflammasome nucleation occurs in large part via homotypic and heterotypic PYD–PYD interactions (21). Such nucleation can be blocked by the binding of PYD-only proteins, which lack other ligand-binding domains (21–23). Our results, which suggest that PYDC3 functions similarly to these other PYD-only proteins, were confirmed using bone marrow-derived macrophages (BMMs) in vitro, in which we found that exogenous expression of PYDC3 suppressed IL1β expression, whereas siRNA-mediated silencing of PYDC3 increased IL1β levels. Collectively, these results identify a previously unknown effect of PGD_2/DP1 signaling in countering deleterious inflammasome activation and, subsequently, ameliorating clinical disease after neurotropic virus infection.

Results

***DP1*$^{-/-}$ Mice Exhibit Decreased Survival After Neurotropic Coronavirus Infection.** MHV causes mild encephalitis with immune-mediated demyelination occurring during virus clearance (24). Given the abundance of PGD_2 in the brain and its anti-inflammatory effects mediated through DP1, we investigated the role of PGD_2/DP1 signaling in the CNS by infecting C57BL/6 (WT) and *DP1*$^{-/-}$ mice with MHV. The absence of DP1 expression increased mortality from 10 to ∼80%, with concomitant weight loss (Fig. 1 *A* and *B*). The virus is detected only in the brain in MHV-infected WT mice (20), but the increased lethality in *DP1*$^{-/-}$ mice was consistent with the notion that virus spread extraneurally in these mice. The liver is a common site of infection in mice infected with many non-JHM strains of MHV (25), but we detected no virus in the livers of infected WT or *DP1*$^{-/-}$ mice at 5 d post infection (dpi) ($n = 4$ or 5 mice per group). Histological examination of WT and *DP1*$^{-/-}$ brains revealed more extensive perivascular inflammation in WT

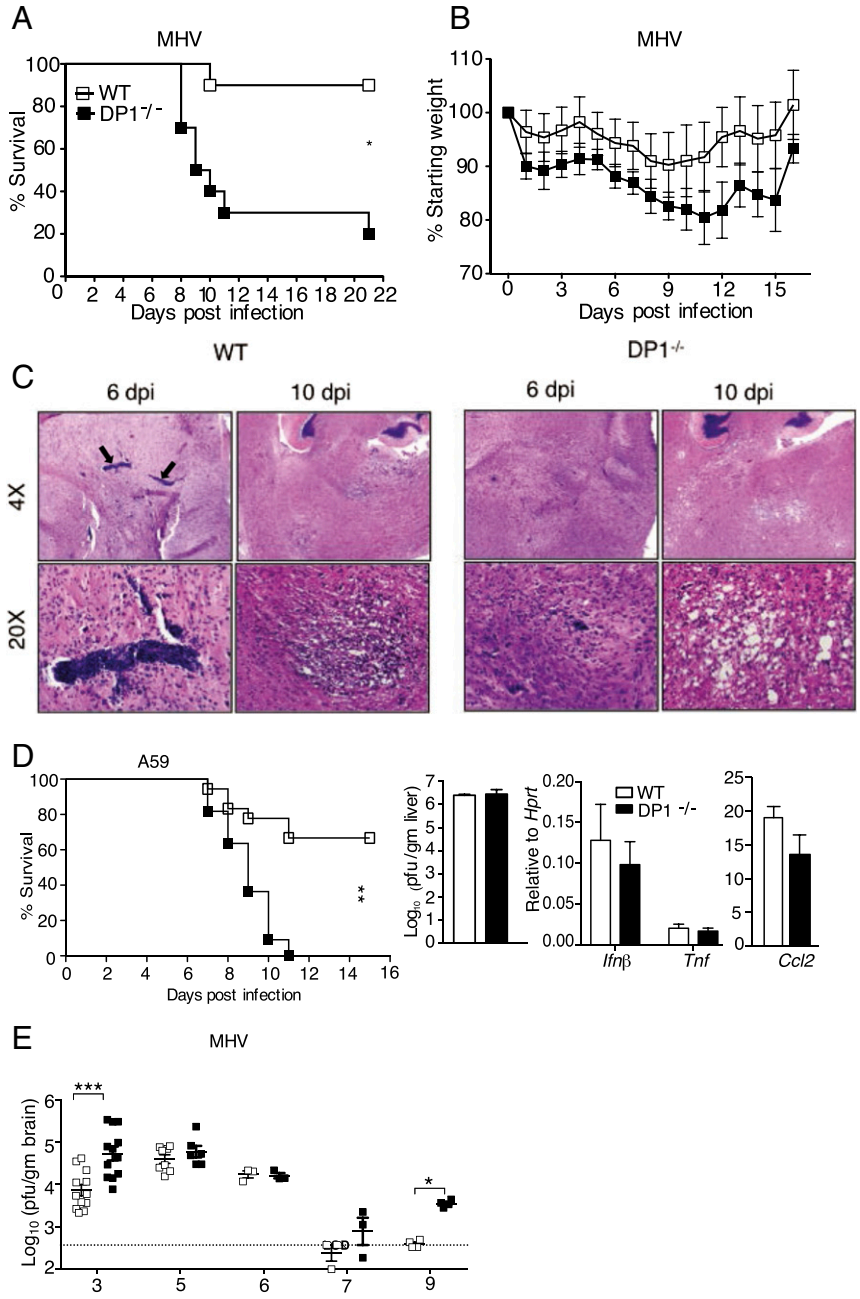

Fig. 1. Increased morbidity and mortality in infected *DP1*$^{-/-}$ mice. Six- to seven-week-old B6 or *DP1*$^{-/-}$ mice were infected i.c. with 700 pfu of MHV (*A*–*D*) or with 3,000 pfu of A59 (*E*). Mice were monitored daily for survival (*A*) and weight loss (*B*) after MHV infection. Data are representative of three independent experiments; $n = 6$ or 7 mice per group. $^*P < 0.05$, Kaplan–Meier log-rank survival test and Student's *t* test. (*C*) Sections from WT and *DP1*$^{-/-}$ brains harvested at 6 and 10 dpi. Arrows indicate large perivascular infiltrates observed at 6 dpi in infected WT but not in *DP1*$^{-/-}$ mice. Data are representative of six to eight mice per group at 5 or 6 dpi and three or four mice per group at 8–10 dpi. (*D*, *Left*) Mice were infected with MHV-A59 and were monitored for survival. Data are representative of two independent experiments; $n = 9$ or 10 mice per group. $^{**}P < 0.01$, Kaplan–Meier log-rank survival test. Virus titers (*Center*) and cytokine mRNAs (*Right*) were measured at 5 dpi. Data represent the mean ± SEM of two independent experiments; $n = 4$ mice per group. (*E*) Viral titers in the brains of MHV-infected B6 or *DP1*$^{-/-}$ mice at indicated time points. Data represent the mean ± SEM of two independent experiments; $n = 4$–10 mice per group. $^*P < 0.05$, $^{***}P < 0.001$, Mann–Whitney *U* test.

mice at 6 and 10 dpi. More remarkably, by 10 dpi, large, multifocal, spongiform lesions were detected in the brainstems of *DP1*$^{-/-}$ mice, whereas mild lesions with monocytic infiltration were present in the same region of WT mice (Fig. 1*C*). To determine whether the requirement for DP1 signaling was confined to the JHM strain of MHV, we infected mice with another neurotropic coronavirus (CoV), the A59 strain of MHV (hereafter, "A59"), which also causes a chronic demyelinating encephalomyelitis with preferential glial cell infection (26). DP1 signaling was also essential in this setting, with survival decreased from 70% in WT mice to 0% in *DP1*$^{-/-}$ mice (Fig. 1*D*). A59 is also hepatotropic, but we observed no differences in virus titers in the liver or in inflammation as assessed by proinflammatory cytokine expression, as is consistent with the CNS being the primary site affected by the absence of DP1 (Fig. 1*D*). Collectively, these results indicate that DP1 signaling was protective in mice infected with two different neurotropic CoVs.

Kinetics of Virus Clearance Is Diminished in *DP1*$^{-/-}$ Mice. To determine whether the absence of DP1 signaling and increased mortality were associated with changes in virus load, we measured MHV titers in the brain at 3–9 dpi (Fig. 1*E*). DP1 signaling was required for initial control of the infection, as shown by increased virus titers at 3 dpi in DP1$^{-/-}$ mice compared with WT mice. Virus titers also were increased at 7 and 9 dpi in DP1$^{-/-}$ mice. The virus-specific T-cell response is required for virus clearance at later times post infection (24), raising the possibility that delayed kinetics of virus clearance reflected a suboptimal T-cell response in the absence of DP1 signaling. However, virus-specific T-cell responses were detected in both WT and *DP1*$^{-/-}$ mice, with *DP1*$^{-/-}$ mice exhibiting higher frequency and numbers of virus-specific CD4 T cells and higher numbers of T_{regs} than WT mice (Fig. S1 *A* and *B*), but WT and *DP1*$^{-/-}$ mice had equivalent numbers of virus-specific CD8 T cells (Fig. S1*C*).

IFN Levels Are Decreased in Infected *DP1*$^{-/-}$ Mice. The significantly higher virus titers at 3 dpi in *DP1*$^{-/-}$ mice were consistent with a suboptimal innate immune response. Because IFN up-regulation is a key component of the anti-MHV host response (27, 28), we examined infected brains for type 1 IFN (IFN-β) mRNA expression. Levels of IFN-β were reduced eightfold in the brains of *DP1*$^{-/-}$ mice compared with WT mice at 3 dpi but not at later times post infection (Fig. 2*A*). To identify the cell type(s) primarily contributing to differences in IFN-β levels at 3 dpi, we sorted brain hematopoietic (CD45^{+}) and nonhematopoietic (CD45^{-}) cells from virus-infected mice (the gating strategy is shown in Fig. S2*A*). IFN-β mRNA was expressed at much lower levels in CD45^{+} but not in CD45^{-} cells from *DP1*$^{-/-}$ compared with WT mice (Fig. 2*B*, *Left*). Further analysis revealed that differences in IFN-β mRNA were confined almost entirely to microglia (Fig. 2*B*, *Right*). In addition, two other antiviral IFNs, IFN-α4 and IFN-λ mRNA, were also diminished in microglia recovered from MHV-infected *DP1*$^{-/-}$ brains (Fig. 2*C*). The differences in IFN-I and IFN-III expression in microglia and the differences in virus loads in the brain could reflect an enhanced susceptibility of *DP1*$^{-/-}$ microglia to virus infection. Although, in agreement with previous results (29), we detected virus in microglia and macrophages (CD11b^{+} cells), we detected no differences in viral loads (viral genomic RNA) in these cells harvested from WT or *DP1*$^{-/-}$ mice (Fig. 2*D*). Consistent with the maximal effects observed at 3 dpi, PGD_2 levels in the brain and *DP1* mRNA expression by CD11b^{+} cells were highest at this time after infection (Fig. 2 *E* and *F*), suggesting that DP1 signaling likely peaked at this time point. Increased PGD_2 expression during CoV infection may result from membrane rearrangements induced during replication, which in turn induce increased activation of upstream phospholipases such as PLA_2G2D (30). We conclude from these findings that PGD_2/DP1 signaling is required for the development of a robust IFN response at early times following neurotropic virus infection.

Microglia Are Less Activated in MHV-Infected *DP1*$^{-/-}$ Mice. Reduced IFN-I and IFN-III expression may have resulted in decreased inflammatory macrophage infiltration into the CNS, but we detected no differences in the frequency and numbers of macrophages and microglia when WT and DP1$^{-/-}$ brains were harvested at 3 dpi and analyzed by flow cytometry (Fig. S2*A*). Reduced IFN expression also suggested that microglia and macrophages were less activated in the absence of DP1 signaling. In agreement with this notion, levels of several activation markers were lower on the surface of *DP1*$^{-/-}$ microglia (CD40, CD86, CD69, F4/80) and macrophages (CD69 and F4/80) (Fig. S2 *B*–*E*). As another measure of activation, we also measured TNF expression in microglia and macrophages directly ex vivo (without exogenous stimulation) in the presence of brefeldin A. The frequency of microglia and, to a lesser extent, of macrophages expressing TNF was diminished in the absence of DP1 signaling (Fig. 3*A*). Additionally, the amount of TNF expressed by microglia on a per cell basis was greater in WT mice than in *DP1*$^{-/-}$ mice (Fig. 3*B*). Differences in numbers of neutrophils could also contribute to outcomes, but we observed no differences in the frequency or numbers of these cells in infected WT and DP1$^{-/-}$ mice (Fig. S2*F*).

These results indicated that the function of both microglia and macrophages was diminished in the absence of DP1 signaling. To distinguish the relative importance of each subset in the poor outcomes in DP1$^{-/-}$ mice, we performed bone marrow chimeras using cells harvested from WT and *DP1*$^{-/-}$ mice with reciprocal transfer into irradiated mice. Unlike macrophages, microglia are radiation resistant and thus are not replaced by the transferred

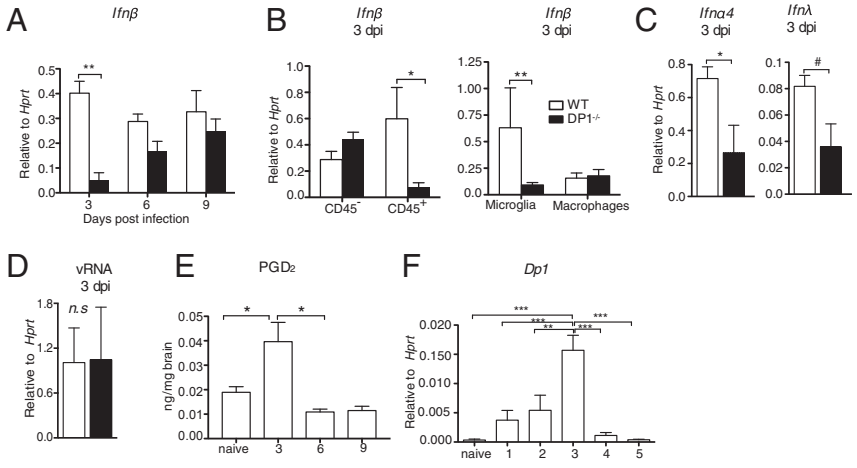

Fig. 2. Blunted IFN-I response in *DP1*$^{-/-}$ mice. WT or *DP1*$^{-/-}$ mice were infected i.c. with MHV, and brains were harvested at the indicated time points post infection for qRT-PCR (*A*–*D* and *F*) and lipid analysis (*E*). (*A* and *B*) *Ifnβ* mRNA expression on days 3, 6, and 9 post infection in total brain (*A*) and in CD45^{-} and CD45^{+} cells (*B*, *Left*) and microglia (CD45^{int}CD11b^{+}) and macrophages (CD45^{hi}CD11b^{+}) (*B*, *Right*) in WT and *DP1*$^{-/-}$ mice at 3 dpi. (*C*) *Ifnα4* (*Left*) and *Ifnλ* (*Right*) mRNA expression in microglia of WT and *DP1*$^{-/-}$ mice. (*D*) MHV RNA levels in microglia and macrophages (CD11b^{+} cells) in the brain at 3 dpi. (*E*) PGD_2 levels in the brains of WT mice measured using LC/MS analysis. (*F*) *Dp1* mRNA levels in CD11b^{+} cells. Data represent the mean ± SEM of two or three independent experiments; $n = 4$ mice per group; $^{*}P < 0.05$; $^{\#}P = 0.053$; $^{**}P < 0.01$; $^{***}P < 0.001$, Mann–Whitney *U* test; n.s., not significant.

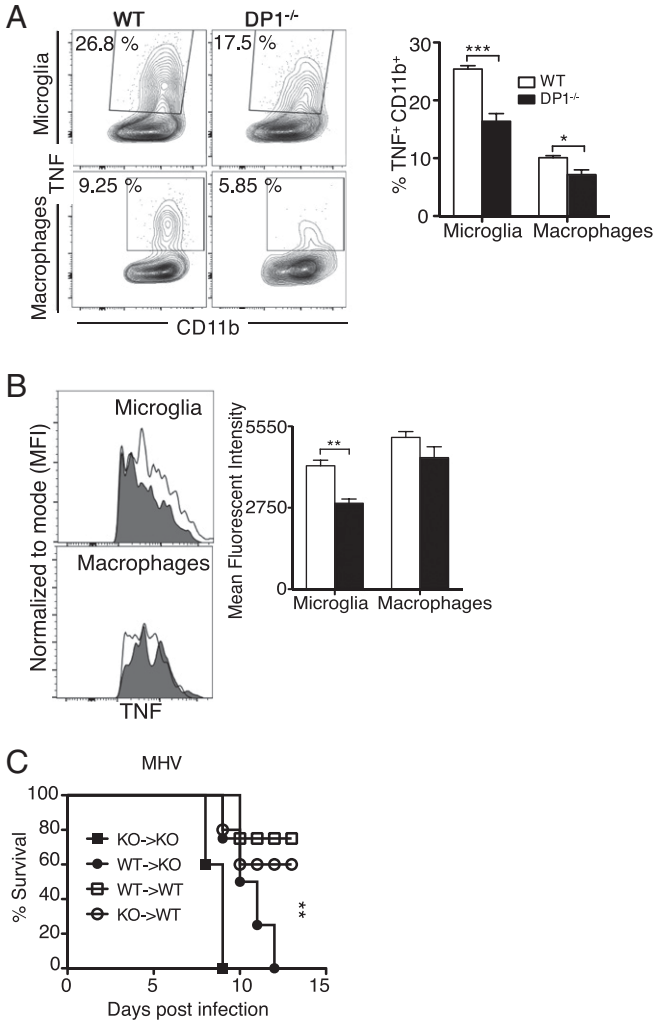

Fig. 3. Decreased microglia and macrophage activation and function in $DP1^{-/-}$ mice. (*A* and *B*) Cells were harvested from the brains of MHV-infected WT or $DP1^{-/-}$ mice on d 3. Functionality of microglia and macrophages are depicted as frequency (*A*) and mean fluorescence intensity (MFI) (*B*) of TNF^+ cells. Data represent the mean ± SEM of two independent experiments; n = 4 mice per group, $^*P < 0.05$; $^{**}P < 0.01$; $^{***}P < 0.001$, Mann–Whitney U test. (*C*) WT and $DP1^{-/-}$ reciprocal bone marrow chimeras were infected with 100 pfu of MHV and monitored for survival. Data represent the mean ± SEM of two independent experiments; n = 7 or 8 mice per group; $^{**}P < 0.01$, Kaplan–Meier log-rank survival test.

bone marrow cells. Independent of the source of donor cells, all recipient $DP1^{-/-}$ mice succumbed to the infection, whereas 60–80% of recipient WT mice were protected (Fig. 3*C*). Thus, DP1 signaling in infiltrating hematopoietic cells was not able to compensate for the lack of DP1 signaling in microglia and perhaps in other CNS-resident cells. Collectively, these data demonstrate that PGD_2/DP1 signaling is required for optimal activation and function of microglia and, to a lesser extent, macrophages.

Abrogation of PGD_2/DP1 Signaling Results in Global Immune Defects in $CD11b^+$ Cells. To understand the global effects of DP1 signaling better, we performed genome-wide expression analysis using sorted brain $CD11b^+$ cells from WT and $DP1^{-/-}$ mice at 3 dpi. Total $CD11b^+$ cells (comprising microglia and macrophages) were used to obtain adequate amounts of RNA. Although 169 genes were differentially regulated in naive WT and $DP1^{-/-}$ CD11b cells, most of these genes either were not annotated or did not fall into specific pathways (Dataset S1).

In contrast, at day 3 after MHV infection, 629 genes were differentially regulated (Dataset S2) in WT vs. $DP1^{-/-}$ cells, with WT cells expressing higher levels of genes involved in immune response pathways among the top pathway/functions identified as differentially regulated by Gene Ontology (GO) enrichment analysis (Fig. 4 *A*–*C*). Among the many genes that were differentially expressed, the gene with maximal fold decrease in $DP1^{-/-}$ $CD11b^+$ cells was *Pydc3* (Dataset S2). Differences in *Pydc3* mRNA levels were confirmed by qRT-PCR analysis (Fig. 4*D*). PYDs in mice and humans have been shown to bind to homologous and heterologous PYDs on proteins, regulating inflammasome function (23, 31). Together, these results suggest that, in addition to effects on generalized microglia and macrophage activation, DP1 signaling likely plays a role in controlling inflammasome activation via PYDC3 up-regulation.

IL-1R Blockade Reversed Lethality in Infected $DP1^{-/-}$ Mice. To address the possibility that there were differences in inflammasome function in WT and $DP1^{-/-}$ mice, we used flow cytometry to measure IL-1β expression and caspase-1 activation by microglia and macrophages following infection. The frequency and numbers of total $CD11b^+$ cells and microglia that expressed IL-1β were significantly higher in $DP1^{-/-}$ mice than in WT mice at 3 dpi (Fig. 5*A*). In addition, IL-1β was expressed at higher levels on a per cell basis in $DP1^{-/-}$ microglia and macrophages (Fig. 5*B*). Another consequence of inflammasome activation is the cleavage of procaspase 1 to its active form, caspase 1. As shown in Fig. 5*C*, activated caspase 1 levels were elevated in total $CD11b^+$ cells and microglia from $DP1^{-/-}$ mice as compared with those levels in total $CD11b^+$ cells and microglia from WT mice, as measured by FAM FLICA binding to active caspase-1 (32).

To probe the role of PYDC3 in inflammasome activation directly, we performed a series of in vitro assays. Our mouse studies indicated that although both microglia and infiltrating macrophages were affected by the absence of DP1 signaling, the effects on the former were considerably greater. However, microglia are notoriously difficult to culture in vitro in sufficient quantities to allow physiological studies, so we chose to use BMMs as a surrogate in subsequent analyses. Because BMMs differ from both microglia and infiltrating macrophages, we first assessed whether they were responsive to DP1 signaling and would therefore be useful for subsequent studies. For this purpose, we infected BMMs with the A59 strain of MHV because cells could be infected at a much higher multiplicity of infection with this virus and because $DP1^{-/-}$ mice were also very susceptible to A59 (Fig. 1*E*). In agreement with the direct ex vivo analyses (Fig. 5 *A* and *B*), levels of secreted IL-1β were significantly greater in $DP1^{-/-}$ BMMs than in WT BMMs at both 12 and 24 h post infection (hpi) (Fig. 5*D*). We also measured levels of a related protein, IL-1α, which is not inflammasome dependent, and found no differences when WT and $DP1^{-/-}$ BMMs were compared at 24 hpi. Because IL-1β induction usually occurs following caspase-1 activation, we performed Western blot analysis and observed higher levels of caspase-1 cleavage in infected $DP1^{-/-}$ than in WT BMMs (Fig. 5*E*).

PGD_2/DP1 signaling has been shown to activate adenyl cyclase, resulting in elevated levels of cAMP. cAMP directly inhibits inflammasome activation (33), so its absence likely contributes to the increased IL-1β production in $DP1^{-/-}$ mice. In agreement with this notion, infection of WT but not $DP1^{-/-}$ BMMs resulted in augmented cAMP levels (Fig. 5*F*), indicating that DP1 signaling is required for cAMP production. When BMMs from mice deficient in various inflammasome components were analyzed for IL-1β expression, we observed that virus-induced IL-1β secretion required an ASC-dependent but NLRP3-independent inflammasome as well as caspase-1 (Fig. 5*G*). These data collectively show that the absence of DP1 resulted in elevated caspase-1 cleavage and IL-1β expression, consistent with heightened inflammasome activation and function.

Finally, we reasoned that if augmented inflammasome activation, and specifically IL-1β signaling, contributed to worse outcomes in

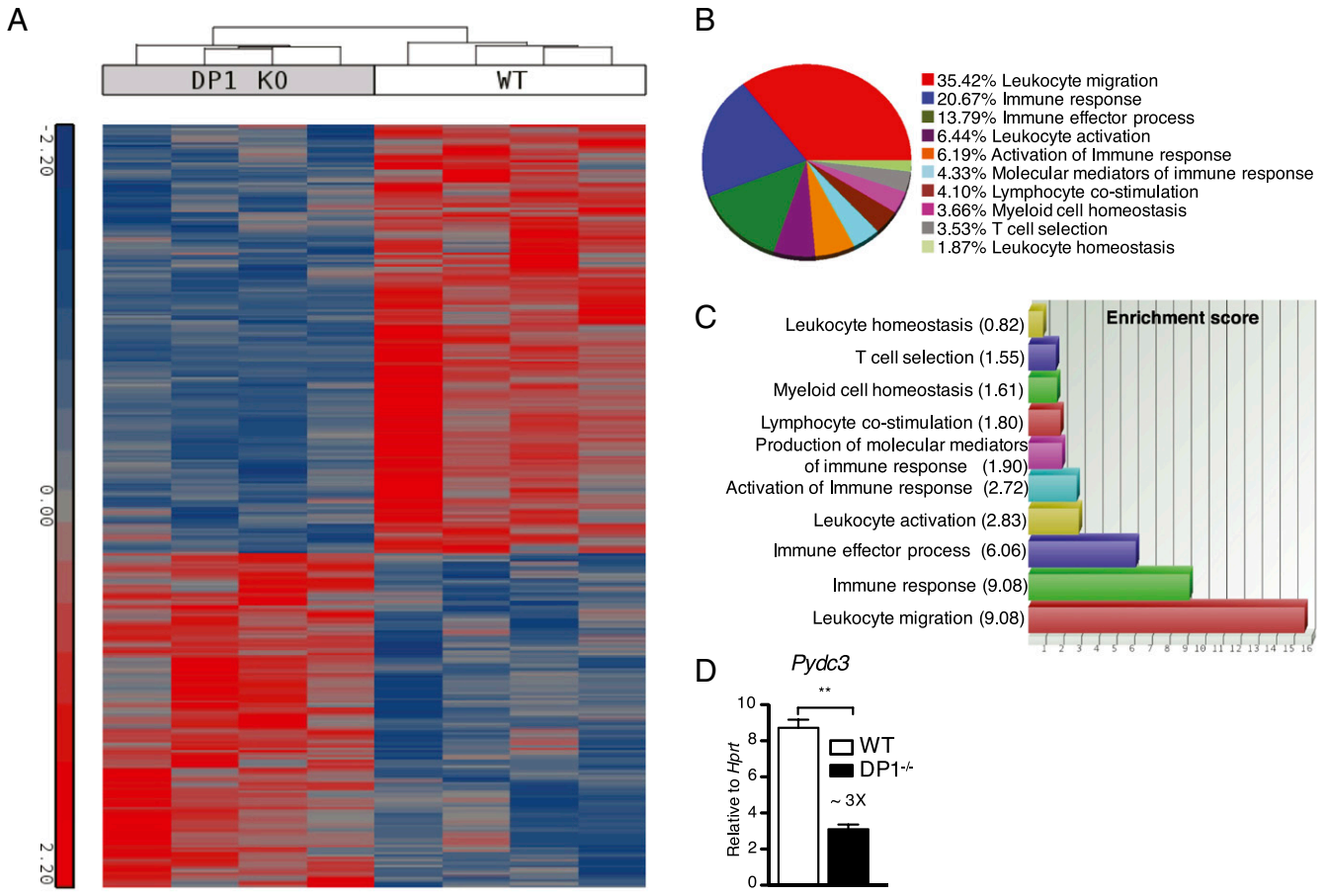

Fig. 4. Microarray analyses of CD11b cells at 3 dpi. *DP1*$^{-/-}$ or WT mice were infected with MHV, and at 3 dpi CD11b^{+} cells from the brain were sorted using magnetic beads for microarray analysis. (*A*) The heat map shows the 629 genes that were differentially regulated between the two groups at a fold-change cut-off of 2 and $P < 0.05$. (*B*) The pie-chart shows the percentage of differentially expressed genes with various immune-related functions. (*C*) The bar graph shows the enrichment score of immune-related genes that were differentially expressed. (*D*) Brain-derived CD11b^{+} cells were sorted from MHV-infected WT and *DP1*$^{-/-}$ mice at 3 dpi and were analyzed for *Pydc3* mRNA levels; $^{**}P < 0.01$.

infected *DP1*$^{-/-}$ mice, treatment with an IL-1 receptor antagonist (i.e., anakinra) would improve survival. Remarkably, treatment with anakinra improved the survival of MHV-infected *DP1*$^{-/-}$ mice from 10 to ~70% (Fig. 5*H*).

Critical Role for Diminished *Pydc3* Expression in Increased Inflammasome Activation. These results demonstrated a role for DP1 signaling in inflammasome suppression but did not address the contribution of PYDC3 to this phenomenon. To address this issue directly, we first showed that treatment with IFN-β induced *Pydc3* expression in both WT and *DP1*$^{-/-}$ BMMs, confirming the IFN-I dependence of PYDC3 expression (Fig. 6*A*). Next, we measured *Ifnβ* and *Pydc3* levels in *DP1*$^{-/-}$ and WT BMMs after virus infection. *Ifnβ* and *Pydc3* were both reduced in A59-infected *DP1*$^{-/-}$ compared with WT BMMs (Fig. 6*B*). To verify that increased *Pydc3* expression was mediated by DP1 signaling, we treated uninfected WT and *DP1*$^{-/-}$ BMMs with BW245C (a DP1 receptor agonist). BW245C enhanced *Pydc3* expression in WT but not in *DP1*$^{-/-}$ BMMs (Fig. 6*C*). Because DP1 signals through cAMP, we next assessed whether direct stimulation of adenyl cyclase, required for cAMP production, circumvented the DP1 signaling requirement for *Pydc3* induction. Treatment of *DP1*$^{-/-}$ BMMs with forskolin, which directly activates adenylate cyclase, resulted in the up-regulation of *Pydc3* mRNA expression in uninfected *DP1*$^{-/-}$ BMMs (Fig. 6*D*). To probe the relative roles of DP1 and IFN-β signaling in PYDC3 expression further, we treated WT or IFN-α receptor double-negative (IFNAR$^{-/-}$) BMMs with BW245C or forskolin. Treatment with either agent resulted in increased PYDC3 expression in WT but not in *ifnar*$^{-/-}$ cells (Fig. 6*E*), indicating that PYDC3 expression is IFN-β dependent, as previously reported (23, 31). Therefore, because BW245C or forskolin treatment resulted in increased PYDC3 expression (Fig. 6 *C* and *D*), we anticipated that IFN-β would also be induced by both treatments. However, contrary to this prediction, IFN-β was not up-regulated in uninfected cells following BW245C or forskolin treatment (Fig. 6*F*). Together, these results indicate that DP1 signaling results in *Pydc3* up-regulation but suggest that this up-regulation occurs only if cells are previously primed for IFN signaling.

Finally, to confirm the role of PYDC3 in inflammasome suppression further, we performed a series of silencing and overexpression assays using A59-infected BMMs. PYDC3 was required for inflammasome suppression because siRNA-mediated knockdown of PYDC3 in WT BMMs resulted in an increase in IL-1β levels (Fig. 6*G*), whereas overexpression of PYDC3 in infected *DP1*$^{-/-}$ BMMs resulted in decreased IL-1β secretion (Fig. 6*H*). Collectively, these data indicate that PYDC3, which is both IFN-I and cAMP inducible, can function to inhibit inflammasome function, thereby suppressing IL-1β secretion.

Key Role for PGD_2/DP1 Signaling in Upregulation of Human POP3. An ortholog of mouse PYDC3 is not encoded in the human genome, but the human protein POP3 (Pyrin only protein 3) may be its functional analog (31). Like PYDC3, POP3 does not contain a DNA-binding HIN domain and has been shown to inhibit inflammasome function (21, 23). To assess the clinical relevance

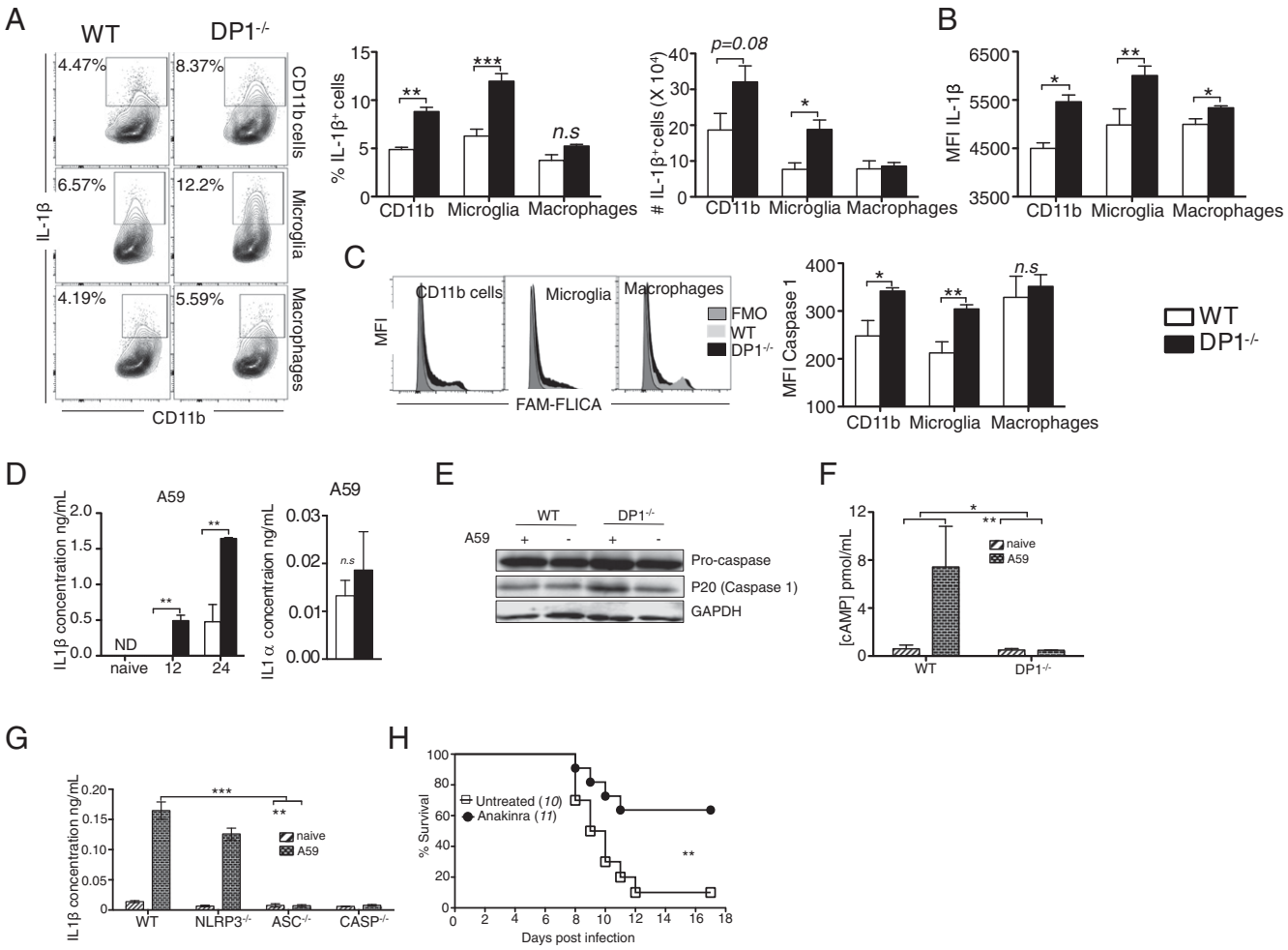

Fig. 5. Increased inflammasome activity in the absence of DP1 signaling. Brain-derived cells from MHV-infected WT or *DP1*$^{-/-}$ mice (*A*–*C*) or BMMs infected with A59 in vitro (*D*–*G*) were analyzed for IL1β (*A*, *B*, *D*, and *G*), caspase-1 (*C* and *E*), or cAMP (*F*). (*A* and *B*) Frequency, number, and MFI (mean fluorescence intensity) of IL-1β–producing total CD11b cells, microglia, and macrophages. (*C*) MFI of activated caspase-1 as shown by FAM-FLICA staining. Data represent the mean ± SEM of two independent experiments; $n = 4$ mice per group; $^{*}P < 0.05$; $^{**}P < 0.01$; $^{***}P < 0.001$, Mann–Whitney *U* test; n.s., not significant. FMO, fluorescent minus one (control). (*D*) Cell supernatants were assayed by ELISA for IL-1β at the indicated time points or IL-1α at 24 hpi. Data represent the mean ± SEM of two independent experiments; $n = 4$ samples per group; $^{**}P < 0.01$, Student's *t* test; n.s., not significant. (*E*) Cell lysates were assayed for caspase 1 activation at 24 hpi by immunoblotting. Data shown are representative of three independent experiments; $n = 2$ samples per group. (*F*) Cell lysates were assayed for cAMP at 24 hpi. Data represent the mean ± SEM of two independent experiments; $n = 4$ samples per group; $^{*}P < 0.05$, $^{**}P < 0.01$, two-way ANOVA. (*G*) BMMs were generated from WT, *NLRP3*$^{-/-}$, *ASC*$^{-/-}$, or *caspase-1*$^{-/-}$ bone marrow and were infected with A59. Cell supernatants were assayed for IL-1β by ELISA at 24 hpi. Data represent the mean ± SEM of two independent experiments; $n = 4$ samples per group; $^{**}P < 0.01$, $^{***}P < 0.001$, two-way ANOVA. (*H*) Six- to eight-week-old DP1$^{-/-}$ mice were treated with anakinra as described in *Materials and Methods*, infected with MHV, and monitored daily. $^{**}P < 0.01$, Kaplan–Meier log-rank survival test. ND, not detected.

of PGD_2 up-regulation of PYDC3, we next determined whether treatment with BW245C or forskolin up-regulated the expression of POP3 in human monocyte-derived macrophages (MDMs). To obtain MDMs, we treated peripheral blood mononuclear cells (PBMCs) with macrophage colony-stimulating factor (M-CSF) for 4 d before treatment with BW245C or forskolin. Induction of DP1 signaling with BW245C (Fig. 6*I*) or induction of cAMP production with forskolin (Fig. 6*J*) resulted in the up-regulation of *Pop3* mRNA, indicating that PGD_2/DP1 signaling in human cells induced POP3. Thus, POP3, like murine PYDC3, could potentially inhibit inflammasome activation in a clinical setting. Consistent with the mouse studies (Fig. 6*E*), neither BW245C or forskolin up-regulated IFN-β expression (Fig. 6 *K* and *L*).

Discussion

Here, we delineate a previously undescribed interaction between PGD_2/DP1 signaling and inflammasome activation in the brain, with the most prominent effects seen in microglia. The mechanism of inflammasome activation in the MHV-infected brain is not well understood, but the ion channel-containing E protein may be involved (34). PGD_2/DP1 signaling resulted in increased expression of IFN-I and PYDC3, helping control excessive inflammasome activation. Although PGD_2, the most abundant prostaglandin in the brain, is produced by brain-resident cells, including microglia, oligodendrocytes, and meningeal cells (17, 35), our results suggested that microglia are a key target for PGD_2. Thus, differences in PYDC3 expression and inflammasome activation were detected to a greater extent in microglia than in infiltrating macrophages. In agreement with microglia, rather than macrophages, having a key role, bone marrow chimera experiments demonstrated that DP1 signaling in nonhematopoietic cells was critical for mouse survival after MHV infection. DP1 is expressed on other cells in the CNS, including astrocytes and neurons (15, 17), so we cannot rule out a role for DP1 signaling in inflammasome activation in these cells. PYDC3 expression is dependent on type I IFN (Fig. 6 *A* and *E*) (23, 31).

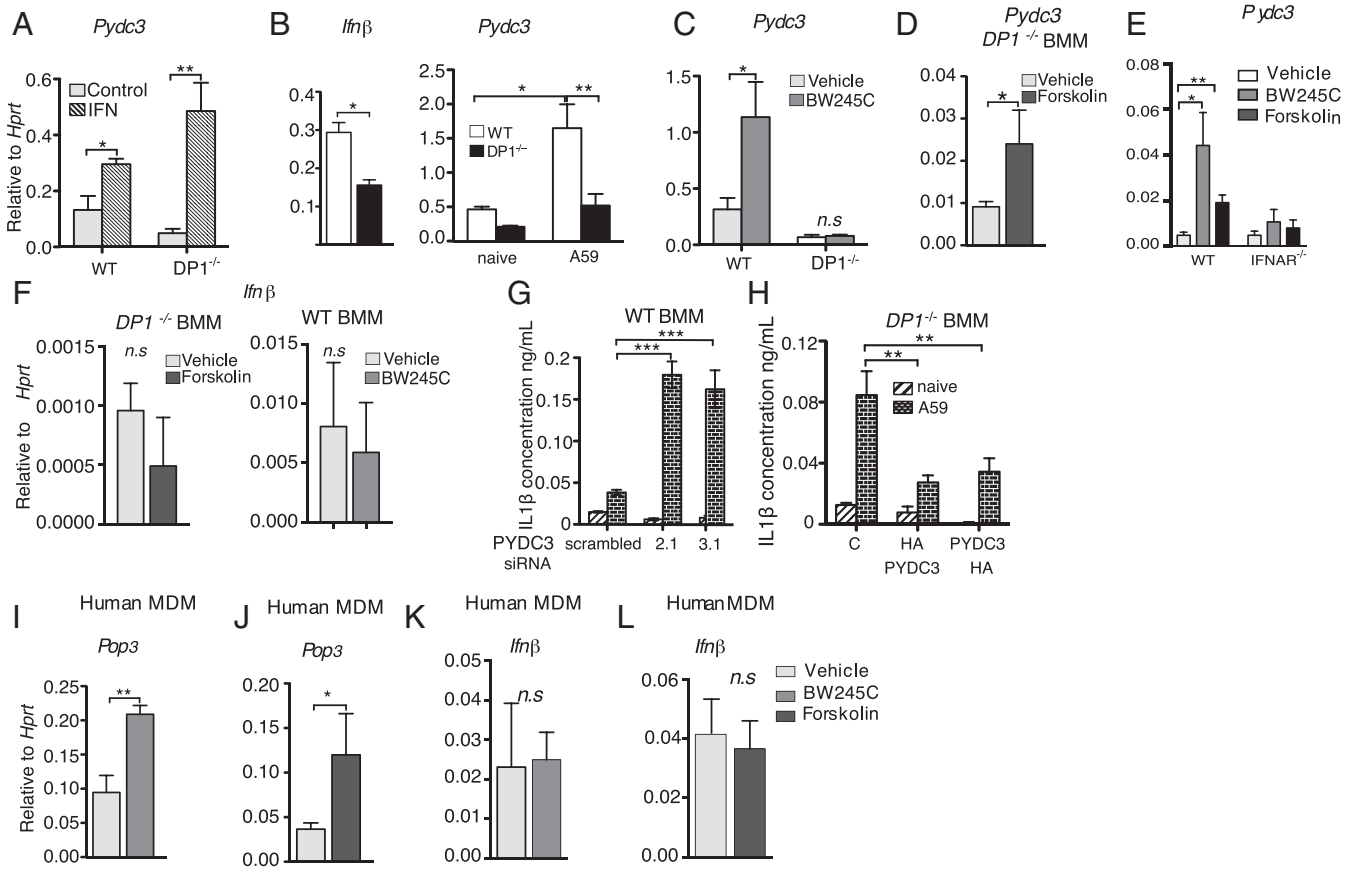

Fig. 6. *Pydc3* inhibits inflammasome function. BMMs from WT, $DP1^{-/-}$, or $IFNAR^{-/-}$ mice (*A–H*) or MDMs from human blood (*I–L*) were prepared. (*A*) *Pydc3* mRNA levels were measured in BMMs treated with IFN-β or PBS (control) for 48 h. (*B*) *Ifnβ* and *Pydc3 mRNA* levels were measured in A59-infected WT or $DP1^{-/-}$ cells. (*C*, *D*, and *F*) *Pydc3* (*C* and *D*) and *Ifnβ* (*F*) mRNA levels were measured in uninfected WT or $DP1^{-/-}$ BMMs following treatment with BW245C (*C* and *F*), forskolin (*D* and *F*), or vehicle for 48 h. (*E*) WT or $IFNAR^{-/-}$ BMMs were treated with BW245C, forskolin, or vehicle, and *Pydc3* mRNA levels were quantified using qRT-PCR. (*G* and *H*) BMMs were infected with A59 following either siRNA-mediated knockdown in WT BMMs (*G*) or overexpression of *Pydc3* in $DP1^{-/-}$ BMMs (*H*), and IL1β in cell supernatants was quantified by ELISA. MDMs were generated from human PBMCs as described in *Materials and Methods*. (*I–L*) *Pop3* (*I* and *J*) or *Ifnβ* (*K* and *L*) mRNA levels following BW245C treatment (*I* and *K*) or forskolin treatment (*J* and *L*) were quantified using qRT-PCR. Data shown represent the mean ± SEM of two independent experiments; $n = 4$ samples per group; $^{**}P < 0.01$; $^{**}P < 0.01$; $^{***}P < 0.001$, Mann–Whitney *U* test; n.s., not significant. MDM, monocyte-derived macrophages.

However, IFN is not up-regulated by forskolin or DP1 agonist treatment (Fig. 6 *F*, *K*, and *L*), indicating that IFN priming is required for PGD_2's effects. Similar requirements for IFN priming were also evident when BMMs infected with Severe Acute Respiratory Syndrome-CoV (SARS-CoV), MHV, or influenza A virus were analyzed for IFN-stimulated gene (ISG) expression (36–39).

PYDC3 has similarities to a family of IFN-I–inducible human proteins, which include POP1, POP2, and POP3. POP family molecules contain a PYRIN domain, lack a sensor domain, and negatively regulate inflammasome activation by inhibiting oligomerization of PYD-containing inflammasome subunits. For example, the PYD of POP3 has extensive (60%) sequence identity with the PYD of the DNA sensor molecule AIM2 and binds to and prevents AIM2 inflammasome activation (22, 23, 31). PYDC3 shares 30% sequence identity with the PYD of ASC, which is required for inflammasome activation in infected cells (Fig. 5*G*), but we were unable to demonstrate any direct physical interaction between the two molecules. In addition, NLRP3 was not required for inflammasome activation (Fig. 5*G*). A previous study showed that transfection with the E protein of a related CoV (SARS-CoV) into Vero cells modestly increased IL-1β release in an NLRP3-dependent manner. These disparate results may reflect differences between infected and transfected cells or between infections with different CoVs.

Other members of the NLRP family contain PYDs, but homology with the PYD of PYDC3 is generally low (less than 20%) (Table S1). Molecules such as NLRC family members and RIG-I are involved in inflammasome formation, but these molecules lack PYRIN domains, making it unlikely that these are PYDC3-binding partners. However, IFI205, MNDA, IFI204, and IFI203 contain PYRIN domains that exhibit 45–60% homology with PYDC3 and are involved in inflammation and apoptosis (40–43). IFI203 and IFI204 are involved in DNA sensing via STING (40, 44). Whether PYDC3 regulates the expression of any of these molecules and their role in the context of an RNA virus infection will require further investigation.

Mortality in $DP1^{-/-}$ mice was mediated in large part by high levels of IL-1β, because survival was increased by anakinra treatment. However, survival was still only 60–70%, suggesting that other consequences of excessive inflammasome activation, including virus-induced pyroptosis, may contribute to disease severity. Pyroptosis has been most commonly studied in cells infected with intracellular bacterial pathogens (45) but also has been shown to result in the destruction of bystander uninfected cells in HIV infection and in the death of monocytes infected with dengue virus (46, 47). Furthermore, reduced levels of IFN-I and IFN-III mRNA in $DP1^{-/-}$ microglia also may have contributed to delayed virus clearance and poor clinical outcomes. Of note, IFN-I directly inhibits inflammasome activation, potentially contributing

to PGD_2-mediated effects (8, 9). IFN-β expression was not induced by DP1 signaling in BMMs, suggesting that the decreased IFN-β levels in microglia in infected mice reflected an indirect consequence of the absence of PGD_2 signaling. Infected *DP1*$^{-/-}$ mice also exhibited increased infiltration of virus-specific CD4 T cells in the brain and histological evidence of diminished perivascular and parenchymal infiltration. These differences may contribute to poor outcomes because, although a robust immune response is required for MHV clearance, virus-specific CD4 T cells have pathogenic as well as protective roles (24, 48, 49). Two- to threefold increases in virus-specific CD4 T cells were shown previously to decrease survival in MHV-infected mice (48). Further, in other models of MHV-induced encephalitis, increased numbers of virus-specific T cells did not result in more rapid kinetics of virus clearance (50), supporting a role for the inflammatory environment in clearance and outcomes independent of the magnitude of the T-cell response.

Although the effect of PGD_2/DP1 signaling on inflammasome activation has not been reported previously, other interactions between inflammasomes and eicosanoids have been described. On one hand, inflammasomes can up-regulate eicosanoid expression, resulting in a hyperinflammatory state with high mortality (2). On the other hand, eicosanoids also may regulate inflammasome activation, but the relationship is complex. Specifically, PGE_2 and PGJ_2 signaling either inhibit or enhance inflammasome activation, depending on the experimental system under study (3–7).

PGD_2/DP1 signaling may be especially important in inflammasome control in the virus-infected brain, but it should be noted that the balance between PGD_2/DP1 signaling and inflammasome function must be finely tuned. In viral encephalitis caused by West Nile virus (WNV), influenza A virus, or HSV, IL-1β is neuroprotective (51–53). In mice lacking ASC expression, WNV levels in the blood and brain were increased, and an exaggerated inflammatory response in the brain was detected (54). Together, these results suggest that PGD_2 expression is increased in MHV-infected mice as a compensatory, proresolving mechanism, partly to restrain excessive inflammasome function, and illustrate a mechanism by which prostaglandin signaling modulates the set-point for an optimal immune response.

Materials and Methods

Mice, Virus, and Infection. Specific pathogen-free 6- to 8-wk-old C57BL/6N mice were purchased from Charles River Laboratories. *DP1*$^{-/-}$ mice were generated as described (55). For infections, mice were lightly anesthetized by administering avertin (300 μL) i.p. and were infected intracranially (i.c.) with 700 or 3,000 pfu of the JHM strain of MHV [rJ2.2, a recombinant version of J2.2-V-1 (20), termed "MHV" herein] or the A59 strain of MHV, respectively, in a 30-μL volume. All animal studies were approved by the University of Iowa Animal Care and Use Committee and meet the stipulations of the *Guide for the Care and Use of Laboratory Animals* (56).

Virus Titration. Brains were harvested on the indicated day post infection. Tissue was homogenized in PBS using a manual homogenizer, and MHV was titered on HeLa-MHVR cells. For plaque assays, cells were fixed with 10% formaldehyde and were stained with crystal violet. Virus titers are expressed as the number of plaque-forming units per gram.

Isolation of Immune Cells from Brains. Brains harvested after PBS perfusion were dispersed and digested with 1 mg/mL collagenase D (Roche) and 0.1 mg/mL DNase I (Roche) at 37 °C for 30 min. Dissociated CNS tissue was passed through a 70-μm cell strainer, followed by Percoll gradient (70/37%) centrifugation. Mononuclear cells were collected from the interphase, washed, and resuspended in culture medium for further analysis. Microglia and macrophages were gated as $CD45^{int}CD11b^{+}$ and $CD45^{hi}CD11b^{+}$, respectively.

Antibodies and Flow Cytometry. The following monoclonal antibodies were used: FITC-, phycoerythrin (PE)-, or PercP Cy5.5-conjugated rat anti-mouse CD45 (30-F11), allophycocyanin (APC)- or e450-conjugated rat anti-mouse CD11b (M1/70), rat anti-mouse CD16/32 (2.4G2), and rat anti-mouse IL1β (NJTEN3) (eBioscience); PercP Cy5.5-conjugated rat anti-mouse I-A/I-E (M5/114.15.2) and APC-conjugated rat anti-mouse TNF (MP6-XT22) (BioLegend); PE- or FITC-conjugated hamster anti-mouse CD80 (16-10A1), PE-conjugated rat anti-mouse CD86 (GL1), and FITC-conjugated rat anti-mouse CD40 (1C 10) (BD Biosciences).

For surface staining, 1×10^6 cells were blocked with 1 μg of anti-CD16/32 antibody and were stained with the indicated antibodies at 4 °C. After washing, cells were fixed using Cytofix Solution (BD Biosciences). To quantify the frequency of cells producing specific cytokines, brain cells were prepared as described above and were incubated in RP10 for 6 h at 37 °C with Brefeldin A and M133 peptide (for virus-specific CD4 T cells) (57), with Brefeldin A (for TNF, $CD11b^{+}$ cells), or without Brefeldin A (for IL1β, $CD11b^{+}$ cells). Cells then were fixed and permeabilized using Cytofix/Cytoperm (BD Biosciences) and were labeled with anti–IFN-γ, anti-TNF, or anti-IL1β antibody. To measure caspase-1 activation, brains cells harvested as described above were incubated with FAM-FLICA reagent (Immunochemistry Technologies) for 1 h at 4 °C. To quantify the frequency and number of virus-specific CD8 T cells, cells were stained with MHC-I/S510 tetramer (National Institute of Allergy and Infectious Diseases Tetramer Core Facility). For Treg quantification, cells were permeabilized using a Foxp3 staining kit (BD Biosciences) and were stained for Foxp3. Flow cytometric data were acquired using a BD FACSVerse flow cytometer and were analyzed using FlowJo software (Tree Star, Inc.).

For cell sorting, brains were harvested at 3 dpi, and a single-cell suspension was prepared as described above. Cells were stained with PercP Cy5.5-conjugated rat anti-mouse CD45 (30-F11) and APC- or e450-conjugated rat anti-mouse CD11b (M1/70) and were sorted using BD FACSDiva.

PCR and Primers. Total RNA was extracted from brain $CD11b^{+}$ cells, microglia ($CD45^{int}$), macrophages ($CD45^{hi}$), or whole brains of naive or MHV-infected mice at the specified time post infection using TRIzol reagent (Invitrogen). Two micrograms of RNA were used for cDNA synthesis. Two microliters of cDNA were added to 23 μL of PCR mixture containing 2× SYBR Green Master Mix (ABI) and 0.2 μM of forward and reverse primers. Amplification was performed in an ABI Prism 7300 thermocycler. Genes and forward and reverse primers are shown in Table S2. Cycle threshold (Ct) values were normalized to those of the housekeeping gene hypoxanthine phosphoribosyltransferase (*HPRT*) by the following equation: $\Delta Ct = Ct_{(\text{gene of interest})} - Ct_{(\text{HPRT})}$. All results are shown as a ratio to *HPRT* calculated as $2^{-(\Delta Ct)}$.

Microarray Analysis. $CD11b^{+}$ cells from the brains of naive or infected (3 dpi) 6- to 8-wk-old WT or *DP1*$^{-/-}$ mice were separated as described above. RNA was purified using a mirVana kit (Life Technologies) according to the manufacturer's instructions. RNA was assessed for purity and quality using an Agilent 2100 Bioanalyzer and was processed using a NuGEN WT-Ovation Pico RNA Amplification System together with a NuGEN WT-Ovation Exon Module. Samples were hybridized and loaded onto Gene Chip mouse gene 2.0 ST arrays (Affymetrix). Arrays were scanned with a HiScan bead array system (Illumina), and data were collected using GeneChip Operating Software (Affymetrix).

Data from Affymetrix Mouse Gene Array 2.0 ST arrays were normalized and median polished using Robust Multichip Average background correction with $\log_2$ adjusted values. After the $\log_2$ expression values for genes were obtained, significance testing was performed comparing the two groups (WT and *DP1*$^{-/-}$). The significance of differences in expression was assessed using a *P* value cutoff of 0.05 and a twofold change. Analysis and visualization of data and pathway analysis were performed using Partek GS software and Ingenuity Pathway Analysis software (QIAGEN Bioinformatics). Complete microarray data have been deposited in the Gene Expression Omnibus [accession numbers GSE84653 (https://www.ncbi.nlm.nih.gov/geo/query/acc.cgi?acc=GSE84653) (naive) and GSE84709 (https://www.ncbi.nlm.nih.gov/geo/query/acc.cgi?acc=GSE84709) (3 dpi)].

LC/MS. Brains were harvested and pulverized in the presence of liquid nitrogen. Seventy milligrams of pulverized brains were mixed with 2 mL of 60% methanol and homogenized using a tissue grinder. The homogenate was incubated for 30 min at 4 °C, and 100 μL (0.1 ng/μL) of internal standard (PGD_2-d4; Cayman Chemicals) was added. Samples were diluted to a final concentration of 10% methanol (vol/vol) with water. Samples were centrifuged at 2,000 × *g* for 10 min, and supernatants were subjected to solid-phase extraction using a Strata-X 33-μm Polymeric Reversed Phase column (60 mg/3 mL; Phenomenex). Columns were activated with 3 mL methanol and washed with 3 mL water. Samples were eluted with 1 mL methanol, vacuum dried, and resuspended in 100 μL of mobile phase A. Analyses were performed using a Waters Acquity triple quadrupole mass spectrometer coupled with liquid chromatography (Acquity H class UPLC). Samples then

were applied to an Acquity UPLC BEH C18 column (130 Å, 1.7 μm, 2.1 mm × 100 mm) and fractionated using a step gradient with mobile phase A (63:37:0.02% water:acetonitrile:formic acid) and mobile phase B (1:1 acetronitrile:isopropanol) at a flow rate of 300 μL/min for most analytes. Primary standards were analyzed in parallel with the samples to enable quantification of the endogenous lipids. Detection of the lipid was performed by multiple reaction monitoring.

Immunoblotting. Total cell extracts were lysed in sample buffer containing SDS, protease, and phosphatase inhibitors (Roche), β-mercaptoethanol, and a universal nuclease (Pierce). Proteins were resolved on a SDS polyacrylamide gel, transferred to a PVDF membrane, hybridized with primary antibody, reacted with an IR dye-conjugated secondary antibody, and visualized using a LI-COR Odyssey Imager (LI-COR). Primary antibodies used for immunoblotting were anti-caspase 1 (Adipogen) and anti-GAPDH (eBioscience). Secondary IR antibodies were purchased from LI-COR.

Bone Marrow Chimera. Bone marrow cells were harvested from femur, tibia, and humerus of WT (Ly5.1 or Ly5.2) or *DP1*$^{-/-}$ (Ly5.2) mice. After RBC lysis, cells were resuspended in PBS at 10^7cells/100 μL of PBS and inoculated i.v. to lethally irradiated 5- to 6-wk-old naive WT (Ly5.1) or *DP1*$^{-/-}$ (Ly5.2) mice. Recipient mice were maintained on an antibiotic diet for 6–8 wk until bone marrow reconstitution.

Anakinra Treatment. Six- to eight-week-old *DP1*$^{-/-}$ mice were treated i.p. with anakinra (Kineret) (10 mg/kg) for 3 d before, on the day of, and 3 d after MHV infection.

Mouse BMMs. WT or *DP1*$^{-/-}$ mice were killed, and femurs were removed. Bone marrow was harvested by flushing with BMM medium (DMEM supplemented with 10% FCS, antibiotics, L-glutamine, and L929-conditioned medium containing mouse M-CSF). The harvested cells were centrifuged at 300 × *g* for 10 min and were treated with ACK lysis buffer (150 mM NH4Cl, 10 mM KHCO3, 0.1 mM Na2EDTA) for 1 min to remove RBCs. ACK lysis buffer was neutralized by adding 10 volumes of PBS, and cells were spun down at 300 × *g* for 10 min. The pelleted cells were resuspended in BMM medium and were plated at 10^6 cells/mL for culture. Medium was replaced on days 4, 5, and 6 of culture before cell use on day 7. In some experiments, BMMs were treated with 20 μM forskolin for 24 h (F6886; Sigma) or with 4 μM BW245C (72814-32-5; Cayman Chemicals) for 48 h.

Plasmids and siRNAs. Codon-optimized *Pydc3* DNA containing both N-terminal and C-terminal HA tags was synthesized (GenScript) and cloned into pcDNA3 plasmid using In-Fusion cloning (Clontech). Plasmids were sequenced before use. For transient expression, plasmids were transfected into BMMs using Amaxa technologies (Lonza) according to the manufacturer's instructions.

To knock down Pydc3 by RNAi, BMMs were transfected with Trilencer-27 siRNAs (OriGene) against *Pydc3* or control siRNA using Lipofectamine 2000 (Life Technologies) according to the manufacturer's instructions. We used two different siRNAs that gave >75% knockdown of the PYDC3 transcript.

Human MDMs. Human peripheral blood samples from leukocyte reduction cones were obtained from anonymous volunteers who had consented to blood donation at the DeGowin Blood Center at the University of Iowa. All protocols involving human samples were approved by the University of Iowa Institutional Review Board. To obtain monocytes, PBMCs were cultured on tissue-culture plates at a seeding density of 1×10^6 cells/mL in RP-10 medium [RPMI medium 1640 (Invitrogen)], with 10% FBS (Atlanta Biologicals) and 2 mM L-glutamine) supplemented with 5 ng/mL M-CSF (eBioscience) at 37 °C with 5% CO_2. After 4 d, the plates were washed with divalent cation-free HBSS (Invitrogen) to remove nonadherent cells. Adherent cells (predominantly MDMs) then were trypsinized and pelleted. Pelleted MDMs were resuspended at 1×10^6 cells/mL in RP10 supplemented with M-CSF (5 ng/mL) and were incubated at 37 °C overnight. MDMs were subsequently seeded at a density of 5×10^5/mL and were incubated for 10 h at 37 °C and 5% CO_2. MDMs then were treated with 20 μM forskolin for 24 h or with 4 μM BW245C for 48 h.

Cytokine and cAMP Quantification. IL-1α and IL-1β quantification was performed by harvesting cell supernatants at the indicated time points and assaying for IL-1α and IL-1β levels using a mouse IL-1α or IL-1β ELISA Ready-Set-Go kit (eBioscience) according to the manufacturer's protocol. For cAMP quantification, cell lysates were harvested in 0.1 M hydrochloric acid, and cAMP levels were assayed following the manufacturer's protocol (cAMP Direct Immunoassay kit; BioVision, Inc.).

Statistics. A Student's *t* test was used to analyze differences in mean values between groups except in the case of the microarray data. All results are expressed as means ± SEM. *P* values less than 0.05 were considered statistically significant; $*P < 0.05$; $**P < 0.01$; $***P < 0.001$. Differences in mortality were analyzed using Kaplan–Meier log-rank survival tests. Microarray data were subjected to two-way ANOVA, and the *P* values used are shown.

ACKNOWLEDGMENTS. We thank Dr. Henry Lin for providing *DP1*$^{-/-}$ mice, Dr. Noah Butler for critically reading the manuscript, and the flow cytometry facility at the University of Iowa for help with sorting. This work was supported in part by NIH Grants R01 NS36592 (to S.P.), R01 AI118719 (to F.S.S.), T32 AI007485 (to A.M.J.), and P30CA086862 (to the flow cytometry facility) and by National MS Society Grant RG5340-A-7 (to S.P.).

1. Ricciotti E, FitzGerald GA (2011) Prostaglandins and inflammation. *Arterioscler Thromb Vasc Biol* 31:986–1000.
2. von Moltke J, et al. (2012) Rapid induction of inflammatory lipid mediators by the inflammasome in vivo. *Nature* 490:107–111.
3. Zoccal KF, et al. (2016) Opposing roles of LTB4 and PGE2 in regulating the inflammasome-dependent scorpion venom-induced mortality. *Nat Commun* 7:10760.
4. Maier NK, Leppla SH, Moayeri M (2015) The cyclopentenone prostaglandin 15d-PGJ2 inhibits the NLRP1 and NLRP3 inflammasomes. *J Immunol* 194:2776–2785.
5. Wang X, et al. (2016) The prostaglandin E2-EP3 receptor axis regulates *Anaplasma phagocytophilum*-mediated NLRC4 inflammasome activation. *PLoS Pathog* 12: e1005803.
6. Mortimer L, Moreau F, MacDonald JA, Chadee K (2016) NLRP3 inflammasome inhibition is disrupted in a group of auto-inflammatory disease CAPS mutations. *Nat Immunol* 17:1176–1186.
7. Sokolowska M, et al. (2015) Prostaglandin E2 Inhibits NLRP3 inflammasome activation through EP4 receptor and intracellular cyclic AMP in human macrophages. *J Immunol* 194:5472–5487.
8. Castiglia V, et al. (2016) Type I interferon signaling prevents IL-1β-driven lethal systemic hyperinflammation during invasive bacterial infection of soft tissue. *Cell Host Microbe* 19:375–387.
9. Guarda G, et al. (2011) Type I interferon inhibits interleukin-1 production and inflammasome activation. *Immunity* 34:213–223.
10. Allan SM, Tyrrell PJ, Rothwell NJ (2005) Interleukin-1 and neuronal injury. *Nat Rev Immunol* 5:629–640.
11. Narumiya S, Ogorochi T, Nakao K, Hayaishi O (1982) Prostaglandin D2 in rat brain, spinal cord and pituitary: Basal level and regional distribution. *Life Sci* 31:2093–2103.
12. Hirai H, et al. (2001) Prostaglandin D2 selectively induces chemotaxis in T helper type 2 cells, eosinophils, and basophils via seven-transmembrane receptor CRTH2. *J Exp Med* 193:255–261.
13. Hervé M, et al. (2003) Pivotal roles of the parasite PGD2 synthase and of the host D prostanoid receptor 1 in schistosome immune evasion. *Eur J Immunol* 33:2764–2772.
14. Saleem S, et al. (2007) PGD(2) DP1 receptor protects brain from ischemia-reperfusion injury. *Eur J Neurosci* 26:73–78.
15. Liang X, Wu L, Hand T, Andreasson K (2005) Prostaglandin D2 mediates neuronal protection via the DP1 receptor. *J Neurochem* 92:477–486.
16. Ahmad AS, Ahmad M, Maruyama T, Narumiya S, Doré S (2010) Prostaglandin D2 DP1 receptor is beneficial in ischemic stroke and in acute exicitotoxicity in young and old mice. *Age (Dordr)* 32:271–282.
17. Mohri I, et al. (2007) Hematopoietic prostaglandin D synthase and DP1 receptor are selectively upregulated in microglia and astrocytes within senile plaques from human patients and in a mouse model of Alzheimer disease. *J Neuropathol Exp Neurol* 66: 469–480.
18. Mohri I, et al. (2006) Prostaglandin D2-mediated microglia/astrocyte interaction enhances astrogliosis and demyelination in twitcher. *J Neurosci* 26:4383–4393.
19. Sawyer N, et al. (2002) Molecular pharmacology of the human prostaglandin D2 receptor, CRTH2. *Br J Pharmacol* 137:1163–1172.
20. Fleming JO, Trousdale MD, el-Zaatari FA, Stohlman SA, Weiner LP (1986) Pathogenicity of antigenic variants of murine coronavirus JHM selected with monoclonal antibodies. *J Virol* 58:869–875.
21. Broz P, Dixit VM (2016) Inflammasomes: Mechanism of assembly, regulation and signalling. *Nat Rev Immunol* 16:407–420.
22. de Almeida L, et al. (2015) The PYRIN domain-only protein POP1 inhibits inflammasome assembly and ameliorates inflammatory disease. *Immunity* 43:264–276.
23. Khare S, et al. (2014) The PYRIN domain-only protein POP3 inhibits ALR inflammasomes and regulates responses to infection with DNA viruses. *Nat Immunol* 15:343–353.
24. Bergmann CC, Lane TE, Stohlman SA (2006) Coronavirus infection of the central nervous system: Host-virus stand-off. *Nat Rev Microbiol* 4:121–132.
25. Masters PS, Perlman S (2013) Coronaviridae. *Fields Virology*, eds Knipe DM, Howley PM (Lippincott Williams & Wilkins, Philadelphia), Vol 1, pp 825–858.
26. Lavi E, Gilden DH, Wroblewska Z, Rorke LB, Weiss SR (1984) Experimental demyelination produced by the A59 strain of mouse hepatitis virus. *Neurology* 34: 597–603.

27. Ireland DD, Stohlman SA, Hinton DR, Atkinson R, Bergmann CC (2008) Type I interferons are essential in controlling neurotropic coronavirus infection irrespective of functional CD8 T cells. *J Virol* 82:300–310.
28. Cervantes-Barragán L, et al. (2009) Type I IFN-mediated protection of macrophages and dendritic cells secures control of murine coronavirus infection. *J Immunol* 182: 1099–1106.
29. Xue S, Sun N, Van Rooijen N, Perlman S (1999) Depletion of blood-borne macrophages does not reduce demyelination in mice infected with a neurotropic coronavirus. *J Virol* 73:6327–6334.
30. Vijay R, et al. (2015) Critical role of phospholipase A2 group IID in age-related susceptibility to severe acute respiratory syndrome-CoV infection. *J Exp Med* 212: 1851–1868.
31. Brunette RL, et al. (2012) Extensive evolutionary and functional diversity among mammalian AIM2-like receptors. *J Exp Med* 209:1969–1983.
32. Grabarek J, Amstad P, Darzynkiewicz Z (2002) Use of fluorescently labeled caspase inhibitors as affinity labels to detect activated caspases. *Hum Cell* 15:1–12.
33. Lee GS, et al. (2012) The calcium-sensing receptor regulates the NLRP3 inflammasome through Ca2+ and cAMP. *Nature* 492:123–127.
34. Nieto-Torres JL, et al. (2015) Severe acute respiratory syndrome coronavirus E protein transports calcium ions and activates the NLRP3 inflammasome. *Virology* 485: 330–339.
35. Beuckmann CT, et al. (2000) Cellular localization of lipocalin-type prostaglandin D synthase (beta-trace) in the central nervous system of the adult rat. *J Comp Neurol* 428:62–78.
36. Zhou H, Zhao J, Perlman S (2010) Autocrine interferon priming in macrophages but not dendritic cells results in enhanced cytokine and chemokine production after coronavirus infection. *MBio* 1:e00219–e00210.
37. Phipps-Yonas H, Seto J, Sealfon SC, Moran TM, Fernandez-Sesma A (2008) Interferon-beta pretreatment of conventional and plasmacytoid human dendritic cells enhances their activation by influenza virus. *PLoS Pathog* 4:e1000193.
38. Kuri T, et al. (2009) Interferon priming enables cells to partially overturn the SARS coronavirus-induced block in innate immune activation. *J Gen Virol* 90:2686–2694.
39. Birdwell LD, et al. (2016) Activation of RNase L by murine coronavirus in myeloid cells is dependent on basal Oas gene expression and independent of virus-induced interferon. *J Virol* 90:3160–3172.
40. Stavrou S, Blouch K, Kotla S, Bass A, Ross SR (2015) Nucleic acid recognition orchestrates the anti-viral response to retroviruses. *Cell Host Microbe* 17:478–488.
41. Zhang K, et al. (2009) Mndal, a new interferon-inducible family member, is highly polymorphic, suppresses cell growth, and may modify plasmacytoma susceptibility. *Blood* 114:2952–2960.
42. Mondini M, et al. (2007) Role of the interferon-inducible gene IFI16 in the etiopathogenesis of systemic autoimmune disorders. *Ann N Y Acad Sci* 1110:47–56.
43. Mondini M, et al. (2010) The interferon-inducible HIN-200 gene family in apoptosis and inflammation: Implication for autoimmunity. *Autoimmunity* 43:226–231.
44. Lee MN, et al. (2013) Identification of regulators of the innate immune response to cytosolic DNA and retroviral infection by an integrative approach. *Nat Immunol* 14: 179–185.
45. Wallach D, Kang TB, Dillon CP, Green DR (2016) Programmed necrosis in inflammation: Toward identification of the effector molecules. *Science* 352:aaf2154.
46. Monroe KM, et al. (2014) IFI16 DNA sensor is required for death of lymphoid CD4 T cells abortively infected with HIV. *Science* 343:428–432.
47. Tan TY, Chu JJ (2013) Dengue virus-infected human monocytes trigger late activation of caspase-1, which mediates pro-inflammatory IL-1β secretion and pyroptosis. *J Gen Virol* 94:2215–2220.
48. Anghelina D, Pewe L, Perlman S (2006) Pathogenic role for virus-specific CD4 T cells in mice with coronavirus-induced acute encephalitis. *Am J Pathol* 169:209–222.
49. Zhao J, Zhao J, Perlman S (2014) Virus-specific regulatory T cells ameliorate encephalitis by repressing effector T cell functions from priming to effector stages. *PLoS Pathog* 10:e1004279.
50. Trujillo JA, Fleming EL, Perlman S (2013) Transgenic CCL2 expression in the central nervous system results in a dysregulated immune response and enhanced lethality after coronavirus infection. *J Virol* 87:2376–2389.
51. Sergerie Y, Rivest S, Boivin G (2007) Tumor necrosis factor-alpha and interleukin-1 beta play a critical role in the resistance against lethal herpes simplex virus encephalitis. *J Infect Dis* 196:853–860.
52. Ramos HJ, et al. (2012) IL-1β signaling promotes CNS-intrinsic immune control of West Nile virus infection. *PLoS Pathog* 8:e1003039.
53. Mori I, et al. (2001) Impaired microglial activation in the brain of IL-18-gene-disrupted mice after neurovirulent influenza A virus infection. *Virology* 287:163–170.
54. Kumar M, et al. (2013) Inflammasome adaptor protein Apoptosis-associated speck-like protein containing CARD (ASC) is critical for the immune response and survival in West Nile virus encephalitis. *J Virol* 87:3655–3667.
55. Matsuoka T, et al. (2000) Prostaglandin D2 as a mediator of allergic asthma. *Science* 287:2013–2017.
56. National Research Council (2011) *Guide for the Care and Use of Laboratory Animals* (National Academies, Washington, DC), 8th Ed.
57. Xue S, Jaszewski A, Perlman S (1995) Identification of a $CD4^+$ T cell epitope within the M protein of a neurotropic coronavirus. *Virology* 208:173–179.